Characterization of microseismic source mechanism in the Marcellus shale through analysis in the spectral domain

Michael J. Nava, James W. Rector, and Zhishuai Zhang, University of California, Berkeley*

Summary

In this paper, we investigate the use of analysis in the spectral domain to overcome the limitations imposed by limited aperture, a common disadvantage to typical monitoring geometry in hydraulic fracturing processes. A typical microseismic monitoring configuration contains two horizontally drilled boreholes – one treatment well and one observation well. This configuration, while cost-effective, leads to an inability to execute moment tensor inversion through traditional means. However, through careful analysis in the spectral domain, parameters like center frequency and bandwidth can be used in tandem with knowledge of process parameters to better understand microseismic source characteristics.

Introduction

There has been a significant increase in the amount of hydraulic fracturing projects in the United States as a result of a number of technical and economic factors. One of the main technological advances that has enabled hydraulic fracturing projects to be completed that were previously economically infeasible is the ability to drill horizontal boreholes. There are many advantages to this approach over the traditional vertical borehole method. For example, a much larger treatment zone in an area of interest can be produced as a direct result of the project geometry. Specifically, due to the orientation of shale formations, a much larger pay zone can be realized by drilling for a greater distance within a horizontal formation.

In order to monitor the microseismic activity resulting from these types of hydraulic fracturing processes, surface arrays or crosswell monitoring arrays are utilized. Surface arrays can be an effective tool for monitoring microseismic since they can provide large azimuthal coverage. However, given that the magnitudes of events resulting from hydraulic fracturing typically range from -1 M_w to -4 M_w, and that the depth of fracturing is usually one or more miles below the surface, signal-to-noise can become a difficult problem to overcome. As such, there is usually the need for both a very large number of acoustic sensors (6,000-24,000 geophones) and a large area at the surface (1-3 miles) to achieve coherent monitoring of microseismic events (Duncan and Eisner 2010).

Downhole monitoring with a horizontal observation well requires significantly fewer acoustic sensors to achieve good signal-to-noise; however, there are also a number of disadvantages to this approach. For example, there is increased uncertainty when determining microseismic event location. This comes as a direct result of the survey geometry. Specifically, since the monitoring array is parallel to the treatment well, location estimates rely on hodogram angle of inclination for depth determination (Maxwell 2014). The main disadvantage of crosswell monitoring, however, is an inability to perform moment tensor inversion with a single monitoring well (Vavryčuk 2007). This constraint is due to the small solid angle as a result from the close proximity of geophones and accompanying limited azimuthal coverage of the treatment zone. This is referred to as the limited aperture problem. In an effort to overcome this restriction, we turn to the spectral domain.

Hydraulic Fracturing Project Overview

The hydraulic fracturing project was performed in Susquehanna County, Pennsylvania in the Marcellus shale formation using the horizontal drilling technique previously discussed. Two horizontal boreholes were drilled – one treatment well and one observation well. The treatment well was used to inject fracture fluid at high pressure in order to exceed the treatment zone's minimum principal stress in an attempt to create new fractures. The newly created fractures increase the permeability and porosity of the zone of interest for the retrieval of hydrocarbon-rich material. A second horizontal borehole was drilled parallel and approximately at the same depth in order to house an array of geophones for measuring acoustic emissions. The treatment well was approximately 5,600 ft in length; the observation well was approximately 4,400 ft in length and the distance between the wells was approximately 720 ft.

There were eighteen fracturing stages in the project progressing from the toe of the well to the heel of the well (Figure 1). In order to monitor the acoustic emissions from microseismic events, the geophone array was moved six times in an effort to minimize viewing distance (Table 1).

Table 1: Description of geophone locations and associated stages.

Hydraulic Fracturing Stage	*Geophone Array Location*
1 - 9	1
10 - 11	2
12 - 13	3
14 - 15	4
16 - 17	5
18	6

DOI http://dx.doi.org/10.1190/segam2015-5911950.1

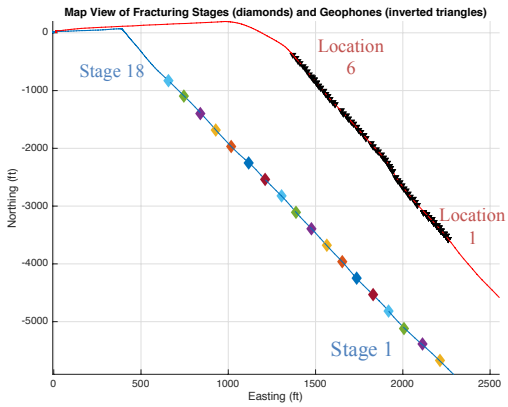

Figure 1: Map view of hydraulic fracturing project in the Marcellus shale. The blue line indicates the treatment well and the red line indicates the observation well. Diamonds represent the average locations of perforations for each of the eighteen stages. Inverted triangles represent the six locations of the geophone array.

Reducing the viewing distance by moving the geophone array is important as it improves signal-to-noise; however, reducing the distance between source and receiver also limits the azimuthal coverage of the events. As such, there is a reduced ability to perform moment tensor inversion as a result of the basic monitoring geometry.

Methods

Analysis of raw data showed many instances of large amplitude ringing. Given that the geophones were not locked into place, or clamped to the borehole casing, these high frequency artifacts were likely caused by tube waves propagating through the borehole (Gaiser 1988). In order to minimize the negative effects of this artifact, low pass and band pass Butterworth filters were applied and a location-based noise characterization and removal schema was developed. This approach considered the root mean square (rms) of each channel of the geophone array for all events. Then the average rms was found for each location of the geophones by only considering the events that occurred at each monitoring location. This is an important step because with each move of the geophone array, the noise signature changes due to a number of factors. For instance, at the first location the geophones could all be oriented in the same manner; however, after being pulled to the next monitoring location, any of the geophones could have shifted in transit. A location-specific approach to noise minimization accounts for these inconsistencies (Figure 2).

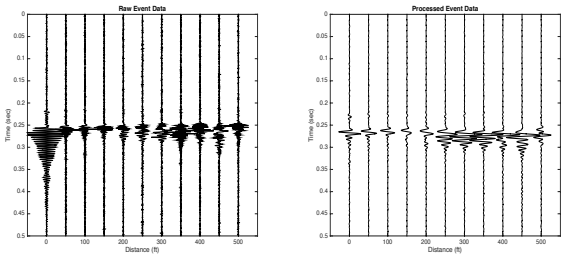

Figure 2: Seismogram showing raw data containing large amplitude artifact believed to be tube wave energy (left) and processed data capturing the same microseismic event (right).

After processing the raw data in order to minimize noise from poor coupling of geophones, first breaks were picked and a 100 ms Tukey (tapered cosine) window was applied to the data in order to capture various waveforms. Specifically, a window to capture compressional waves, a window to capture shear waves, and also a combined window capturing both waveforms were applied to the processed data. This approach gives information regarding the spectral content of each waveform and also the overall event for later analysis.

A Fourier Transform was performed on the three windowed wave types for each trace, which yielded a spectral response for each of the eleven geophones. In order to reduce the amount of data to interpret, an average spectral response of all traces for each event was calculated to show a representative spectral response on a total event basis.

With a representative spectral response for each event, we begin to focus on properties like bandwidth and center frequency to gain some intuition regarding relationships between event spectra and source mechanism. In order to classify bandwidth, the global maximum of each signal was identified and the associated prominence calculated. At one-half the prominence, the width of the signal is noted. This is done for all event spectra and we are left with a relative measure of bandwidth for the three wave types. An example of a broadband and a narrowband event are shown in Figure 3.

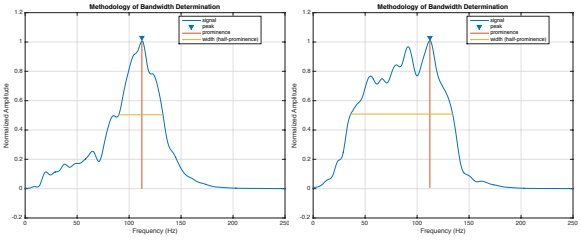

Figure 3: Determination of bandwidth. Inverted triangle represents global maximum, vertical line shows prominence of the signal, and

DOI http://dx.doi.org/10.1190/segam2015-5911950.1

horizontal line represents the width measured at one-half the prominence.

Additionally, the center frequency for each event was determined using the centroid method (Bracewell 1965). In order to find the frequency at which the majority of the signal energy is located, the first moment, or centroid, of the event spectra is found by:

$$f_c \overset{\text{def}}{=} \langle x \rangle = \frac{\int_{-\infty}^{\infty} x f(x) dx}{\int_{-\infty}^{\infty} f(x) dx}$$

An understanding of where the signal energy is located in the frequency domain is important as it can give information about slip distance, Q determination, and other source parameters (Beresnev 2001; Brune 1970, 1971; Eaton 2011, 2014; Maxwell 2011). With bandwidth and center frequency measurements for windowed compressional waves, windowed shear waves, and also a combined window, event characteristics can be seen.

Results

As a preliminary step, the mean center frequency and mean bandwidth were calculated in order to see if there were apparent statistical trends in the data. Compressional wave mean center frequency and bandwidth are lower then the shear wave parameters. Furthermore, the combined window mean center frequency and bandwidth are both closer to the mean of the shear wave (Table 2). As such, it can be inferred that the majority of microseismic energy may be associated with shear openings and less from tensile events.

Table 2: Mean values of bandwidth and center frequency for the three types of applied windows.

	Mean Bandwidth (Hz)	*Mean Center Frequency (Hz)*
Compressional Wave	61.9	86.0
Shear Wave	72.5	92.3
Combined Window	66.0	88.6

Considering the event spectra, we see that there is a large amount of variation between events throughout the hydraulic fracturing project (Figure 4a). After sorting these event spectra by bandwidth, it can be seen that there is still variation within narrowband events (Figure 4b). Finally, after sorting event spectra by center frequency, less variation can be seen (Figure 4c). Moreover, in this last view, it is evident that the majority of broadband events are located near the middle of the range. This is due to the fact that the centroid method considers the frequency at which the majority of signal energy is located. As such, broadband events typically have center frequencies near the mean.

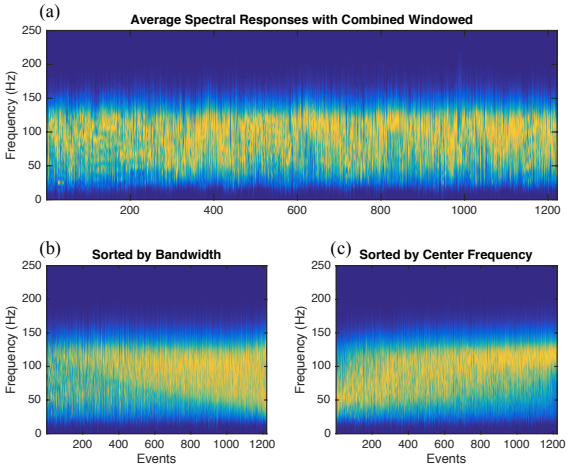

Figure 4: Combined window event spectra for all events in the hydraulic fracturing project. Color represents normalized amplitude where blue is lowest and yellow is greatest. Unsorted events (top) show large variation between neighboring events. Bandwidth-sorted events (bottom left) show variation between narrowband events. Center frequency-sorted events (bottom right) show broadband events located in the middle – near the mean

In an effort to more effectively interpret the data, scalar values of center frequency and bandwidth were plotted as a function of time. This enabled correlation between spectral properties and process parameters like surface pressure, slurry flow rate, and proppant concentration. Figure 5 and Figure 6 show spectral and process parameters as a function of time.

Interesting relationships can be seen between both bandwidth and center frequency when compared to event magnitude in the seventh stage of the hydraulic fracturing project. For example, there is an indication that bandwidth has an inverse relationship with event magnitude. As such, there is an implication that narrowband events are accompanied by greater magnitude. Additionally, center frequency appears to vary proportionally to magnitude. Consequently, it seems that events with the largest magnitude are narrowband events with high center frequencies.

DOI http://dx.doi.org/10.1190/segam2015-5911950.1

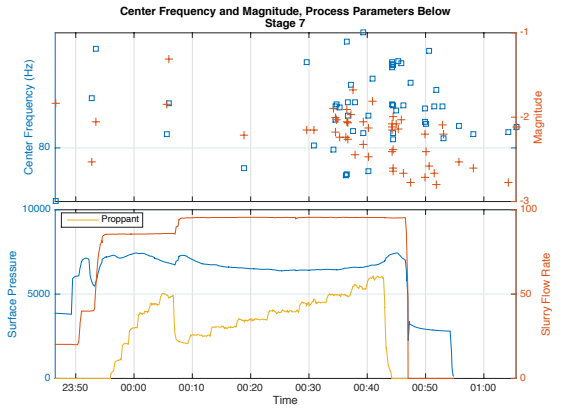

Figure 5: Center frequency (blue square) and event magnitude (red plus) as a function of time shown on top. Hydraulic fracturing process parameters – surface pressure (blue), slurry flow rate (red), and proppant concentration (yellow) are shown on the bottom.

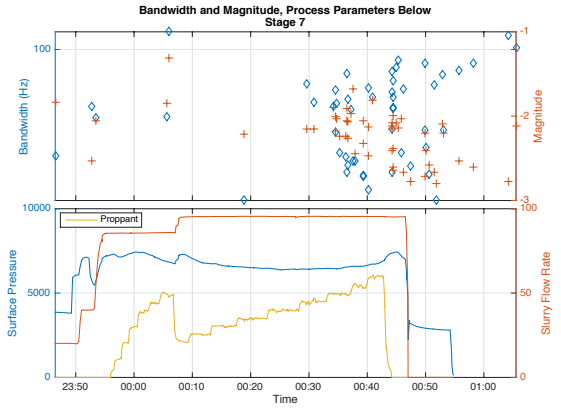

Figure 6: Bandwidth (blue diamond) and event magnitude (red plus) as a function of time shown on top. Note that at the end of the stage, it is clear that there is an inverse relationship between bandwidth and magnitude. Process parameters are same as above.

Another method of analysis is similar to the S/P amplitude ratio method traditionally used to understand source mechanism. Here, the event bandwidth is considered. In an effort to determine the main component of source energy, we investigate the ratio of windowed shear wave bandwidth to windowed compressional wave bandwidth. Since the mean bandwidth was higher for shear waves and lower for compressional waves, we conclude that a larger bandwidth ratio indicates a shear wave dominated event. Conversely, a lower bandwidth ratio would indicate that the event is dominated by compressional energy. A spatial plot displaying the locations of microseismic events is shown where color and size both indicate S/P bandwidth ratio (Figure 7).

While it may be difficult at this stage to determine whether high shear regions exist, it is possible to better understand fault plane orientation in the area of interest (Warpinski 2010). Despite the limitations imposed on source mechanism determination as a result of survey geometry, shear and compressional wave-dominated events are seen distributed throughout the treatment zone.

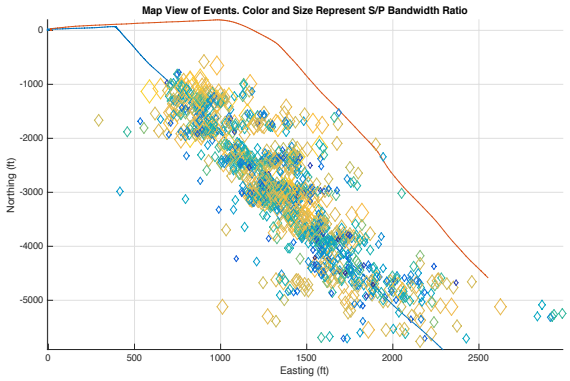

Figure 7: Map view of treatment zone. Diamonds indicate locations of microseismic events. Color and shape both represent S/P bandwidth ratio, where blue is smallest and yellow is largest. Large, yellow diamonds represent shear-dominated events.

Conclusions

In an effort to overcome the restrictions imposed on moment tensor inversion as a result of a single monitoring array configuration, analysis in the spectral domain is performed. Preliminary analysis reveals relationships between spectral parameters and both source and process characteristics. For example, after windowing compressional and shear waves, compressional waves are, in general, more narrowband in nature. Shear waves are predominately broadband events with a higher center frequency. Considering the ratio of these determined parameters gives an indication of events dominated by shear energy, which may lead to a better understanding of shear opening events in the treatment zone.

Acknowledgements

The authors would like to acknowledge support from RPSEA under contract 11122-20.

DOI http://dx.doi.org/10.1190/segam2015-5911950.1

EDITED REFERENCES

Note: This reference list is a copyedited version of the reference list submitted by the author. Reference lists for the 2015 SEG Technical Program Expanded Abstracts have been copyedited so that references provided with the online metadata for each paper will achieve a high degree of linking to cited sources that appear on the Web.

REFERENCES

Beresnev, I. A., 2001, What we can and cannot learn about earthquake sources from the spectra of seismic waves: Bulletin of the Seismological Society of America, **91**, no. 2, 397–400. http://dx.doi.org/10.1785/0120000115.

Bracewell, R., 1965, The Fourier transform and its applications: McGraw-Hill.

Brune, J. N., 1970, Tectonic stress and the spectra of seismic shear waves from earthquakes: Journal of Geophysical Research, **75**, no. 26, 4997–5009. http://dx.doi.org/10.1029/JB075i026p04997.

Brune, J. N., 1971, Correction: Journal of Geophysical Research, **76**, 5002.

Duncan, P. M., and L. Eisner, 2010, Reservoir characterization using surface microseismic monitoring: Geophysics, **75**, no. 5, 139–146.

Eaton, D. W., 2011, Q-determination, corner frequency and spectral characteristics of microseismicity induced by hydraulic fracturing: 81st Annual International Meeting, SEG, Expanded Abstracts, http://dx.doi.org/10.1190/1.3627499.

Eaton, D. W., 2014, Magnitude, scaling, and spectral signature of tensile microseisms: EGU General Assembly Conference Abstracts, 16.

Gaiser, J. E., T. J. Fulp, S. G. Petermann, and G. M. Karner, 1988, Vertical seismic profile sonde coupling: Geophysics, **53**, 206–214. http://dx.doi.org/10.1190/1.1442456.

Mawell, S., 2014, Microseismic imaging of hydraulic fracturing: Improved engineering of unconventional shale reservoirs: SEG, 17. http://dx.doi.org/10.1190/1.9781560803164.

Maxwell, S. C., 2011, What does microseismic tell us about hydraulic fracture deformation: CSEG Recorder, **36**, no. 8, 31–45.

Vavryčuk, V., 2007, On the retrieval of moment tensors from borehole data: Geophysical Prospecting, **55**, no. 3, 381–391. http://dx.doi.org/10.1111/j.1365-2478.2007.00624.x.

Warpinski, N. R., and J. Du, 2010, Source-mechanism studies on microseismicity induced by hydraulic fracturing: SPE Annual Technical Conference and Exhibition. http://dx.doi.org/10.2118/135254-MS.